



## 2Mg–Fe alloys processed by hot-extrusion: Influence of processing temperature and the presence of MgO and MgH<sub>2</sub> on hydrogenation sorption properties

Gisele F. de Lima<sup>a</sup>, Sebastiano Garroni<sup>b</sup>, Maria D. Baró<sup>b</sup>, Santiago Suriñach<sup>b</sup>, Cláudio S. Kiminami<sup>c</sup>, Walter J. Botta<sup>c</sup>, Mauricio M. Peres<sup>c</sup>, Alberto M. Jorge Junior<sup>c,\*</sup>

<sup>a</sup> PPGCEM, Federal University of São Carlos, São Carlos, SP, Brazil

<sup>b</sup> Fac. Sciences, Edifici Cc Universitat Autònoma de Barcelona, 08193 Bellaterra, Spain

<sup>c</sup> Department of Materials Engineering, Federal University of São Carlos, Via Washington Luiz, km 235, 13565-905 São Carlos, SP, Brazil

### ARTICLE INFO

#### Article history:

Received 1 July 2010

Received in revised form 3 November 2010

Accepted 5 November 2010

Available online 13 November 2010

#### Keywords:

2Mg–Fe alloy

Hot extrusion

Hydrogen storage

### ABSTRACT

2Mg–Fe alloy powder produced by high-energy ball milling was processed by hot extrusion at temperatures of 200 °C and 300 °C to produce bulk samples. The alloys were hydrogenated for 24 h under hydrogen pressures of 24 bar (to produce the Mg<sub>2</sub>FeH<sub>6</sub> phase) and 15 bar (to produce a mixture of MgH<sub>2</sub> + Mg<sub>2</sub>FeH<sub>6</sub> phases), respectively. After the hydrogenation treatments, the complex hydride Mg<sub>2</sub>FeH<sub>6</sub> was identified in both conditions, while the MgH<sub>2</sub> and MgO phases were observed only after extrusion at 200 °C. Desorption temperatures varied with the extrusion conditions; extrusion at 300 °C resulted in a desorption onset temperature about 68 °C lower than that of samples extruded at 200 °C, and about 200 °C lower than that of commercial MgH<sub>2</sub>. Extrusion at the lower temperature did not change the number of stored defects (point defects, dislocations, voids, stacking faults, vacancies and others) produced in the milling process and increased the preferential sites for hydride nucleation, increasing the hydrogen storage capacity. The presence of MgO produced the beneficial effect of grain boundary pinning, but delayed the onset temperature of desorption. The combined presence of MgH<sub>2</sub> and Fe after hydrogenation at 15 bar seems to play a catalytic role that considerably hastened the Mg–H reactions and increased the desorption kinetics. However, the desorption kinetics in both conditions was still low.

© 2010 Elsevier B.V. All rights reserved.

### 1. Introduction

Magnesium and Mg-based alloys are promising materials for hydrogen storage in the solid state due to their efficiency in mass and volume of storage, their safety, since the decomposition of hydrides is an endothermic process, and also their easier handling at ambient temperature than other storage methods. Among the metallic-based hydrides, magnesium hydride (MgH<sub>2</sub>) has the highest gravimetric storage capacity (~7.6 wt% of H), and the ternary intermetallic Mg<sub>2</sub>FeH<sub>6</sub> has a high capacity of 5.5 wt% of H and the highest volumetric storage capacity of 150 kg/l of H, which is almost double that of liquid hydrogen. However, for possible practical applications, the hydrogen sorption rates of Mg/Mg-based alloy need to be faster than that observed for crystalline Mg-based hydrides, the temperatures for these reactions should decrease, and also the reactivity toward air and oxygen should be lower [1]. With the development of nanostructured materials processed by high-energy ball milling (HEBM) in the 1990s, reasonable sorption

kinetics was observed in Mg-based hydrides [2]. The addition of catalyst elements and the formation of nanocomposite materials also contributed to enhance the H-sorption kinetics [3].

Before the complex hydride Mg<sub>2</sub>FeH<sub>6</sub> was synthesized by Didisheim in 1984 [4], iron was added to magnesium to catalyze the reactions with hydrogen, as an additive to prevent agglomeration of Mg particles, and to improve cyclability [5]. The addition of Fe to MgH<sub>2</sub> was also found to improve the hydrogen absorption properties, but not the hydrogen desorption kinetics [6]. Further studies focused on the synthesis of the complex Mg<sub>2</sub>FeH<sub>6</sub> hydride [7]. More recently, the different techniques of severe plastic deformation (SPD) have been also used in the development of Mg-based hydrides [8–9]. SPD and thermomechanical processing are methods that can result in important grain refinement and can also be used to consolidate powders into bulk samples that should be more resistant to air than the equivalent materials obtained by conventionally high energy ball milling. All the most common SPD techniques, such as high pressure torsion (HPT) [8], accumulative roll bonding (ARB) [9] and equal channel angular pressure (ECAP) [10], have been used in Mg and Mg alloy processing. These SPD techniques applied to Mg-based systems have resulted in improved hydrogen sorption properties and kinetics.

\* Corresponding author. Tel.: +55 16 33518531; fax: +55 16 33615404.

E-mail address: [moreira@dema.ufscar.br](mailto:moreira@dema.ufscar.br) (A.M. Jorge Junior).

In this paper we report on the results obtained from 2Mg–Fe alloy samples processed by hot-extrusion at two different temperatures. The extruded alloy samples were initially produced by means of high-energy ball milling and subsequently consolidated by hot-extrusion. The hydrogenation properties of the samples extruded in different conditions were also investigated.

## 2. Experimental

Pure magnesium (+20–100 mesh, 99.98%, Alfa Aesar) and Fe (–20 mesh, 99.998%, Alfa Aesar) were mixed into the 2Mg–Fe (at.%) composition by means of high-energy ball milling, using a ball-to-powder ratio of 20:1 under argon gas atmosphere in a Fritsch P7 planetary ball mill for 12 h. The powder was sieved using an 80 mesh sieve.

Cold-pressed preforms were produced using powders with particle sizes of up to 180  $\mu\text{m}$ . To analyze the influence of extrusion temperature, the preforms were then hot-extruded under the following conditions: ram speed of 1 mm/min, extrusion ratio of 3/1 (to ensure a high level of porosity) and extrusion temperatures of 200 °C and 300 °C (extrusion condition 1 and 2, respectively, which are referred to hereinafter as Ext-S-1 and Ext-S-2).

The bulk samples produced in both conditions were then hydrogenated at 400 °C for 24 h in a reactor under hydrogen pressures of 24 bar to produce the  $\text{MgH}_2$  phase [11] and 15 bar to produce only  $\text{Mg}_2\text{FeH}_6$  [11] (hereinafter referred to as Ext-S-1-PCT and Ext-S-2-PCT).

The microstructure was characterized by scanning electron microscopy (Philips XL30 and Jeol JSM-6300) and transmission electron microscopy (FEI-CM120).

The phases were identified by X-ray diffraction (XRD) using monochromatic Cu-K $\alpha$  radiation with an angular pass of 0.032° in a Rigaku DMAX diffractometer equipped with a C-monochromator.

Rietveld refinement was used to analyze the XRD spectra and determine the crystallite size, and to identify phases and phase proportions, using Maud software [12]. The thermal and thermogravimetric properties of the extruded samples were analyzed using a Netzsch Simultaneous Thermal Analyzer (STA) 449 Jupiter calorimeter, which can take simultaneous differential scanning calorimetric (DSC) and thermogravimetric (TG) measurements and quadrupole mass spectrometer (QMS) Aeolos equipment.

Hydrogen desorption temperatures were measured during continuous heating of the hydrides at a constant heating rate of 10 °C/min, using purified and dried argon gas in an overflow regime.

## 3. Results and discussion

Cold-pressing to produce the preforms resulted in relative densities of around 0.51, which were basically maintained after extrusion, suggesting that the temperatures we used had no effect on porosity. XRD patterns of the 2Mg–Fe alloys processed by hot-extrusion and of the powders revealed the presence of hcp-Mg and bcc-Fe.

Fig. 1 shows the XRD patterns of extruded samples after heat treatment to absorb hydrogen; Fig. 1(a) extrusion at 200 °C and treatment at 24 bar of  $\text{H}_2$ , and Fig. 1(b) extrusion at 300 °C and treatment under a pressure of 15 bar of  $\text{H}_2$ . A comparison of the peak intensities in the XRD patterns indicated that the amount of hydride phases was larger in the samples extruded under condition 1, i.e., at the lower temperature. The phases were indexed and their weight percentages were estimated during the Rietveld refinement, using Maud software. In Ext-S-1-PCT, extruded at 200 °C and hydrogenated under 24 bar of  $\text{H}_2$ , the analysis indicated, with absolute error lower than 3%, 12.1 wt% of  $\alpha$ -Mg, 26.7 wt% of Fe, 2.8 wt% of  $\text{MgH}_2$ , 47.9 wt% of  $\text{Mg}_2\text{FeH}_6$ , and 10.5 wt% of  $\text{MgO}$ .

For extrusion at 300 °C and hydrogenation under 15 bar of  $\text{H}_2$  these values were: 36.9 wt% of  $\alpha$ -Mg, 43.4 wt% of Fe, and 19.7 wt% of  $\text{Mg}_2\text{FeH}_6$ . Obviously, the higher hydrogen mass capacity observed in the first processing condition is due to the higher hydrogen pressure applied and the phases formed are in accordance with the phase diagram presented in reference [11]. However, the residual iron at same applied pressure can be calculated based on the ideal gas law. In this context, the residual iron would be 27.1 wt% for sample Ext-S-2-PCT against 26.7 wt% of Fe in Ext-S-1-PCT, i.e., the absorption capacity of Ext-S-1-PCT continues to be higher than that of Ext-S-2-PCT. These differences will be discussed later.

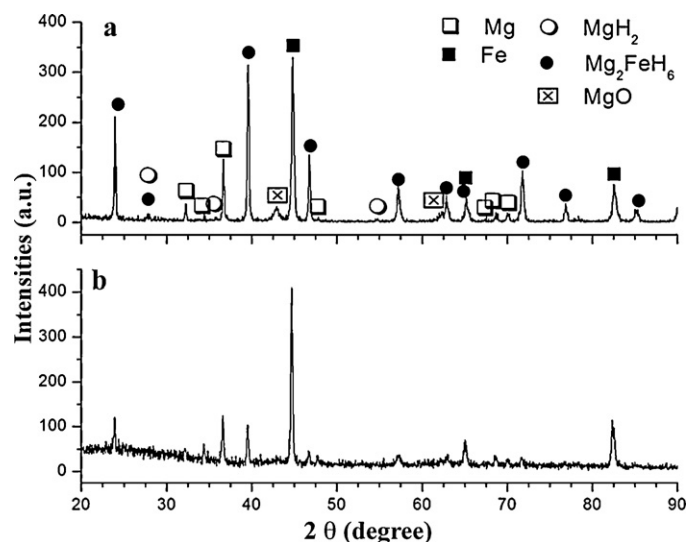


Fig. 1. XRD patterns of the samples extruded and treated by hydrogen absorption in the following conditions: (a) extrusion at 200 °C and treatment under a pressure of 24 bar of  $\text{H}_2$  and (b) extrusion at 300 °C and treatment under a pressure of 15 bar of  $\text{H}_2$ .

Fig. 2 shows further results of Rietveld refinement from the XRD patterns. The microstrain data (Fig. 2(a)) indirectly reveal that the samples processed at 200 °C maintained and increased the largest number of defects produced during milling (such as point defects, dislocations, voids, stacking faults, vacancies and others), probably, in this temperature condition, the recovery process could not be completed.

When the specimen was extruded at 300 °C, deformation occurred easily and the softening processes acted more effectively, decreasing the number of defects in the crystalline structure. This behavior was reproduced when the samples were hydrogenated at higher temperatures, i.e., due to recovery from defects, the microstructural strain was reduced. Also, as expected and as shown in Fig. 2(b), the crystallite sizes increased with annealing, hot-extrusion or hydrogenation treatment. However, even with this increase, the nanosize range was maintained, a fact that was attributed to the pinning effect of the iron at the Mg grain boundary, preventing Mg grain growth. In addition, it is interesting to note, as observed by other authors [13], the beneficial effect of grain boundary pinning by magnesium oxide particles in combination with Fe, as occurred in the sample extruded at 200 °C.

Together with the thermodynamic effects produced by the difference in pressure, which produced the  $\text{MgH}_2$  and  $\text{Mg}_2\text{FeH}_6$  in sample Ext-S-1-PCT, already observed by Bogdanovic et al. [11], another important point that can be inferred from the above discussion is that the greater number of defects in samples extruded at 200 °C could cause an increase in the number of preferential nucleation sites for hydride phases. This would explain the differences in hydrogen absorption properties indicated by the hydrogen absorption calculated indirectly from the residual iron after correction of the pressure, as mentioned above.

Fig. 3(a) and (c) shows BSE-SEM images and Fig. 3(b) and (d) TEM-BF images of samples processed in the two conditions, i.e., extrusion at 200 °C and hydrogenation under 24 bar and extrusion at 300 °C and hydrogenation under 15 bar, respectively.

The main features that can be observed in Fig. 3 are (i) regions of untransformed Mg + Fe, where the pale gray matrix is Mg and the white dots are Fe; (ii) regions of hydride + Fe (dark gray ring-shaped region); and (iii) TEM-BF images confirm the nanosize of the particles in both cases. The Fe pinning effect is clearly visible in the BSE-SEM images, and the Fe catalyst effect will be discussed later.

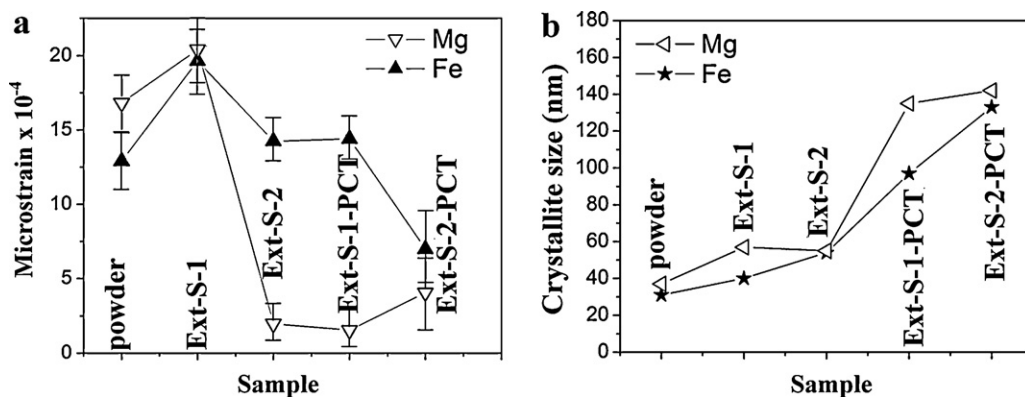


Fig. 2. Values estimated in the Rietveld refinement of XRD patterns: (a) microstrains and (b) crystallite sizes.

Fig. 4 shows STA results of the hydrogenated samples. Fig. 4(a) shows the desorption temperatures of extruded samples compared with commercial  $\text{MgH}_2$  powder. The onset and peak temperatures of Ext-S-1-PCT and Ext-S-2-PCT occurred at 293–447 °C and 225–431 °C, respectively. Both samples presented lower onset temperatures than the commercial  $\text{MgH}_2$  powder, i.e., about 127 °C and 195 °C lower for Ext-S-1-PCT and Ext-S-2-PCT, respectively. Fig. 4(b) shows sigmoidal curves obtained from the numeric integration of Fig. 4(a) and normalized for 100% of transformation. This figure shows the incubation time and the kinetic behavior of the two samples.

From Fig. 4(b) it is possible to observe that the desorption kinetics of these samples are still slow, mainly due to the bulk form of the analyzed samples when compared to the  $\text{MgH}_2$  powders. As a result, the peak desorption temperatures, observed in Fig. 4(a), are very close to that of commercial  $\text{MgH}_2$ . The data observed indicate

an incubation time prior to the onset of dehydrogenation. As this figure shows, the incubation time of sample Ext-S-2-PCT is longer than for sample Ext-S-1-PCT, which can be explained by the presence of  $\text{MgO}$  in this sample, despite its beneficial pinning effect, as discussed earlier.

The results depicted in Fig. 4(a) and (b) indicate that the addition of Fe and the presence of  $\text{MgH}_2$  is expected to significantly reduce the dissociation barriers for  $\text{H}_2$  dissociation as well as the onset temperature of dehydrogenation, when compared with  $\text{MgH}_2$ .

This might indicate that the dissociation of  $\text{H}_2$  and recombination of H to  $\text{H}_2$  mainly occur in association with iron due to its lower barrier compared to that of pure magnesium, even in the presence of a very small percentage of Fe. This may suggest that Fe catalyzes mainly the dissociation/recombination reaction barrier for  $\text{H}_2$  and has a minor influence on other processes. Moreover, Fig. 4(b) also shows the faster dehydrogenation kinetics of

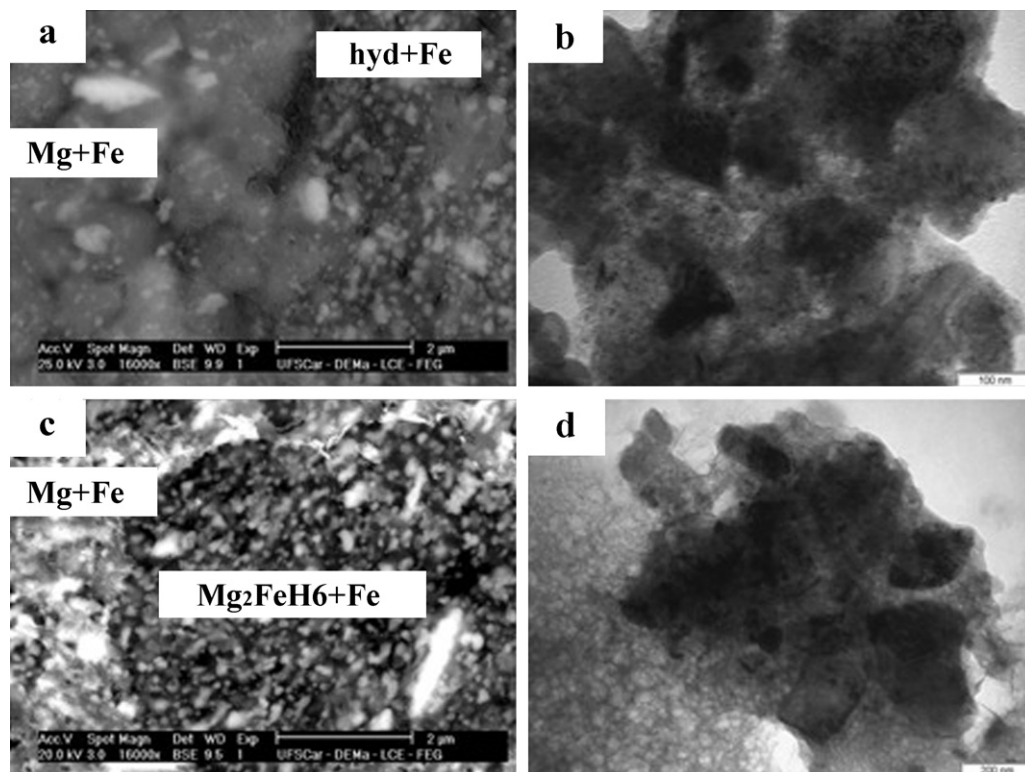
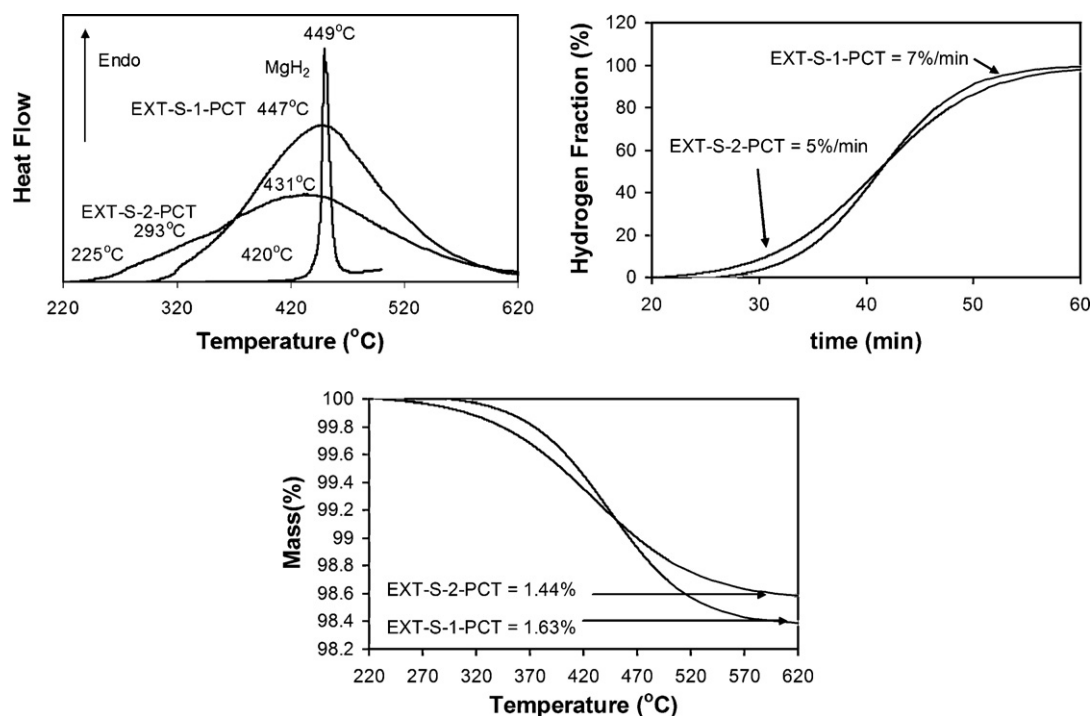


Fig. 3. (a) FEG-SEM image (BSE mode) of Ext-S-1-PCT; (b) TEM image of Ext-S-1-PCT; (c) FEG-SEM image (BSE mode) of Ext-S-2-PCT; and (d) TEM image of Ext-S-2-PCT.



**Fig. 4.** STA measurements: (a) differential scanning calorimetry; (b) sigmoidal curves obtained from (a), showing the incubation time and the kinetic behavior of the two samples. (The values of 7%/min and 5%/min were obtained from the slope of the linear region of (b) and represent the maximum desorption rate.) (c) Thermogravimetric analyses (TGAs) showing that Ext-S-1-PCT stored a higher percentage of hydrogen (1.63 wt% of H) than Ext-S-2-PCT (1.44 wt% of H).

the Ext-S-1-PCT samples, which is visible (7%/min for Ext-S-1-PCT and 5%/min for Ext-S-2-PCT, these values were obtained from the slope of the linear region of Fig. 4(b) and represent the maximum rate of desorption) along with the sigmoidal curves. Here, the combined effect of  $\text{MgH}_2$  and iron in sample Ext-S-1-PCT seems to play a catalytic role, considerably hastening the Mg–H reactions in an apparently more efficient way than when only iron is employed for this same purpose.

The thermogravimetric analyses (TGA) (Fig. 4(c)) confirmed the DRX findings that Ext-S-1-PCT stored a higher percentage of hydrogen (1.63 wt% of H) than Ext-S-2-PCT (1.44 wt% of H), and with higher kinetics. As discussed earlier, the higher hydrogen storage capacity and faster desorption kinetics of Ext-S-1-PCT are attributed to the combination of  $\text{MgH}_2$  and Fe and to the larger number of defects in this sample.

#### 4. Conclusions

Extrusion performed at a lower temperature maintained the number of stored defects produced in the milling process and increased the preferential sites for hydride nucleation, increasing the hydrogen storage capacity.

The presence of  $\text{MgO}$  resulted in beneficial grain boundary pinning, but delayed the onset temperature of desorption.

The combined effect of  $\text{MgH}_2$  and iron in the sample hydrogenated at lower pressure seems to play a catalytic role, considerably hastening the Mg–H reactions and increasing the desorption kinetics.

#### Acknowledgements

The authors gratefully acknowledge the financial support of FAPESP, CAPES and CNPq (Brazil), and of the European Commission under MRTN-Contract “Complex Solid State Reactions for Energy Efficient Hydrogen Storage” (MRTN-CT-2006-035366).

#### References

- [1] B. Sakintuna, F. Lamari-Darkrimb, M. Hirscher, *Int. J. Hydrogen Energy* 32 (2007) 112–1140.
- [2] S. Rivoirard, P. Rango, D. Fruchart, J. Charbonnier, D. Vempaire, *J. Alloys Compd.* 356–357 (2003) 622–625.
- [3] J.F.R. Castro, A.R. Yavari, A. Lemoulec, T.T. Ishikawa, W.J. Botta, *J. Alloys Compd.* 389 (2005) 270–274.
- [4] J.J. Didisheim, P. Zolliker, K. Yvon, P. Fischer, J. Schefer, M. Gubelmann, A.F. Williams, *Inorg. Chem.* 23 (1984) 1953–1957.
- [5] J.-M. Welter, P.S. Rudman, *Scr. Metall.* 16 (1982) 285–286.
- [6] G.F. Lima, A.M. Jorge Jr., D.R. Leiva, C.S. Kiminami, C. Bolfarini, W.J. Botta, *J. Phys.: Conf. Ser.* 144 (2009) 012015, doi:10.1088/1742-6596/144/1/012015.
- [7] S. Li, R.A. Varin, O. Morozova, T. Khomenko, *J. Alloys Compd.* 384 (2004) 231–248.
- [8] Y. Kusadome, K. Ikeda, Y. Nakamori, S. Orimo, Z. Horita, *Scr. Mater.* 57 (2007) 751–753.
- [9] T.T. Ueda, M. Tsukahara, Y. Kamiya, S. Kikuchi, *J. Alloys Compd.* 386 (2005) 253–257.
- [10] V. Skripnyuk, E. Buchman, E. Rabkin, Y. Estrin, M. Popov, S. Jorgensen, *J. Alloys Compd.* 436 (2007) 99–106.
- [11] B. Bogdanovic, A. Reiser, K. Schlichte, B. Spliethoff, B. Tesche, *J. Alloys Compd.* 345 (2002) 77–89.
- [12] L. Lutterotti, R. Ceccato, R. Dal Maschio, E. Pagani, *Mater. Sci. Forum* 87 (1998) 278–281.
- [13] K.-F. Aguey-Zinsou, T. Nicolaisen, J.R. Ares Fernandez, T. Klassen, R. Bormann, *J. Alloys Compd.* 434–435 (2007) 738–742.